ISSN 0030-400X, Optics and Spectroscopy, 2021, Vol. 129, No. 5, pp. 681–687. © Pleiades Publishing, Ltd., 2021.

SPECTROSCOPY OF CONDENSED MATTER

Atomic Structure and Optical Properties of Plasma Enhanced Chemical Vapor Deposited SiCOH Low-*k* Dielectric Film

V. N. Kruchinin[a, *], V. A. Volodin[a, b], S. V. Rykhlitskii[a], V. A. Gritsenko[a, b, c], I. P. Posvirin[d], Xiaoping Shi[e], and M. R. Baklanov[f, g]

[a] *Rzhanov Institute of Semiconductor Physics, SB RAS, Novosibirsk, 630090 Russia*
[b] *Novosibirsk State University, Novosibirsk, 630090 Russia*
[c] *Novosibirsk State Technical University, Novosibirsk, 630073 Russia*
[d] *Boreskov Institute of Catalysis SB RAS, Novosibirsk, 630090 Russia*
[e] *Beijing Naura Microelectronics, E-Town, Beijing, China*
[f] *North China University of Technology, Beijing, China*
[g] *Russian Technological University MIREA, Moscow, Russia*
**e-mail: vladd.kruch@yandex.ru*

Received October 6, 2020; revised December 3, 2020; accepted December 26, 2020

Abstract—The SiCOH low-*k* dielectric film was grown on Si substrate using plasma-enhanced chemical vapor deposition method. Atomic structure and optical properties of the film were studied with the use of X-ray photoelectron spectroscopy (XPS), Fourier transform infrared (FTIR) absorption spectroscopy, Raman spectroscopy, and ellipsometry. Analysis of XPS data showed that the low-*k* dielectric film consists of Si–O_4 bonds (83%) and Si–SiO_3 bonds (17%). In FTIR spectra some red-shift of Si–O–Si valence (stretching) vibration mode frequency was observed in the low-*k* dielectric film compared with the frequency of this mode in thermally grown SiO_2 film. The peaks related to absorbance by C–H bonds were observed in FTIR spectrum. According to Raman spectroscopy data, the film contained local Si–Si bonds and also C–C bonds in the s–p^3 and s–p^2 hybridized forms. Scanning laser ellipsometry data show that the film is quite homogeneous, homogeneity of thickness is ~2.5%, and homogeneity of refractive index is ~2%. According to the analysis of spectral ellipsometry data, the film is porous (porosity is about 24%) and contains clusters of amorphous carbon (~7%).

Keywords: low-*k* dielectrics, PECVD, optical properties, atomic structure

DOI: 10.1134/S0030400X21050088

INTRODUCTION

Low dielectric constant (low-*k*) materials have been introduced into ultra-large-scale integration (ULSI) technology together with low resistivity Cu interconnections starting from the end of 1990s to reduce signal propagation delay in interconnects (RC-delay), crosstalk noise, and power consumption [1, 2]. They replaced traditional SiO_2 dielectric and Al conductors that were used in early generations of ULSI devices. Different low-*k* materials from organic polymers to metal-organic framework were evaluated during the past 20 years [3]. Each low-*k* material has certain advantages and disadvantages, but carbon-doped oxides (also termed as SiCOH and organosilica glasses) deposited by plasma-enhanced chemical vapor deposition (PECVD) were selected as the most suitable candidates, at least for technology nodes ≥7 nm. The most important reason for this selection is that they have properties relatively similar to traditional SiO_2 and also can be deposited by using the same equipment as for SiO_2 deposition. Therefore, integrated circuit (IC) manufacturers do not need to adapt principally new equipment (as in the case of chemical solution deposition) and it reduces the cost of implementation.

In this work, PECVD SiCOH low-*k* dielectric developed for sub 45 nm technology nodes is studied. The goal of this work is to study the atomic structure and optical properties of these films, correlate them with chemical composition.

EXPERIMENTAL PART

SiCOH low-*k* dielectrics were PECVD deposited by using diethoxymethylsilane (DEMS) as a network matrix precursor and alpha-terpinene (ATRP) as a precursor of a sacrificial porogen [4–6]. Both molecules (matrix and porogen precursors) were simulta-

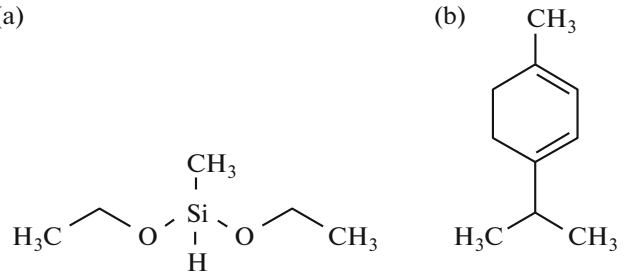

Fig. 1. Structure of the used precursors; (a) diethoxymethylsilane (DEMS), (b) alpha-terpinene (ATRP).

neously introduced into the plasma reactor and transformed into species that eventually led to the formation of a "hybrid" film composed of an organosilicate-based matrix enclosing organic inclusions. Then, during a post-deposition treatment such as ultraviolet (UV) assisted thermal curing, the organic phase, consisting of the porogen molecule fragments, was removed. A broadband UV source with wavelength >200 nm was used for the curing. After complete curing at $T \approx 400$°C, the film became porous and had ultra-low-k properties. Figure 1 shows the structure of precursors used for the deposition of the studied low-k film.

For studying the atomic structure of the deposited low-k film the X-ray photoelectron spectroscopy (XPS) was used. The X-ray photoelectron spectra were measured using SPECS spectrometer with a PHOIBOS-150-MCD-9 analyzer and FOCUS-500 monochromator (Al$K\alpha$ radiation, $h\nu$ = 1486.74 eV, 200 W). The binding energy (BE) scale was pre-calibrated using the positions of the peaks of Au $4f_{7/2}$ (BE = 84.0 eV) and Cu $2p_{3/2}$ (BE = 932.67 eV) core levels. The peaks BE was calibrated by the C1s peak position (284.8 eV), corresponding to the surface hydrocarbon-like deposits [7]. The survey spectrum and the narrow spectra were registered at the analyzer pass energy 20 eV. Atomic ratios of the elements were calculated from the integral photoelectron peak intensities, which were corrected by corresponding sensitivity factors based on Scofield photoionization cross-sections [8]. The analysis of the data obtained by XPS was carried out by the software of XPS Peak 4.1 [9]. The sample's surface was etched with Ar^+ ions with the energy of 1.25 keV at the current density of 8–10 μA cm^{-2} for 10 min using an IQE 11/35 ion gun. The depth profiling rate under these conditions was estimated as 0.5 nm/min.

The chemical composition of low-k film was studied by using vibrational spectroscopy methods. The presence of nonpolar chemical bonds in the films was detected from analysis of the Raman spectroscopy data. Raman spectra were recorded at room temperature in the backscattering geometry using Ar^+ laser for excitation, wavelength is 514.5 nm. The Raman spectrometer T64000 (Horiba Jobin Yvon) was used. Incident light was linearly polarized; the polarization of scattered light was not analyzed. The silicon charge-coupled device (CCD) matrix, cooled with liquid nitrogen, was used as a photodetector. The spectral resolution was not worse than 2 cm^{-1}. An attachment based on an Olympus microscope was used for microscopic analysis of the Raman spectra. The power of the laser beam at the sample was about 1 mW. To avoid local heating of the films by laser beam, the sample was placed slightly further than the focus and the spot size was 20 μm. The polar chemical bonds were studied using Fourier transform infrared (FTIR) absorption spectroscopy. FT-801 spectrometer (SIMEX analytical equipment) having 4 cm^{-1} spectral resolution was used.

The porosity of the film was studied by using ellipsometric porosimetry. The experimental tool, measurement, and calculations procedure was described in detail in our recent publication [10]. For this, the optical properties of the low-k film in visible, near IR and UV regions were studied using laser scanning (He–Ne laser, $h\nu$ = 1.96 eV) and spectral ellipsometry. For laser scanning ellipsometry studies the Microscan-3M (Institute of Semiconductor Physics SB RAS, Russia) setup was used [11], angle of incidence of the laser beam was 60°. An ELLIPS-1891-SAG (Institute of Semiconductor Physics SB RAS, Russia) spectral ellipsometer was used for ellipsometric analysis of the thin films on nontransparent silicon substrates [12]. The spectral dependences of ellipsometric angles $\Psi(h\nu)$ and $\Delta(h\nu)$ were measured in the range 1–5 eV. The spectral resolution of the device was about 0.01 eV, the angle of light incidence was 70°. A four-zone measurement technique was used and averaging was performed over all four zones.

RESULTS AND DISCUSSION

Figure 2 shows Si2p photoelectron spectra of the low-k dielectric film, spectra of thermally grown SiO_2 and low-k dielectric film after Ar^+ bombardment are also presented for comparison. The impact of argon ions was local both in area (several square microns) and in depth; the ions change the structure of the film at a depth of 2 nm.

In this work, upon deconvolution of the Si2p level peak, we assume, as in most works [13, 14], that the number of possible components corresponding to the oxidation states of silicon: 0, 1+, 2+, 3+, 4+ does not exceed 5. One can see that stoichiometric thermally grown SiO_2 consists only of Si–O_4 bonds (Si^{4+} level on Fig. 2). Si2p level deconvolution shows that the low-k dielectric film consists of Si–O_4 bonds and Si–SiO_3 bonds (Si^{3+} level in Fig. 2). Bombardment of low-k dielectric results in decreasing of Si^{4+} fragment concentration and creation of Si^{2+} fragments (Si–Si_2O_2 bonds).

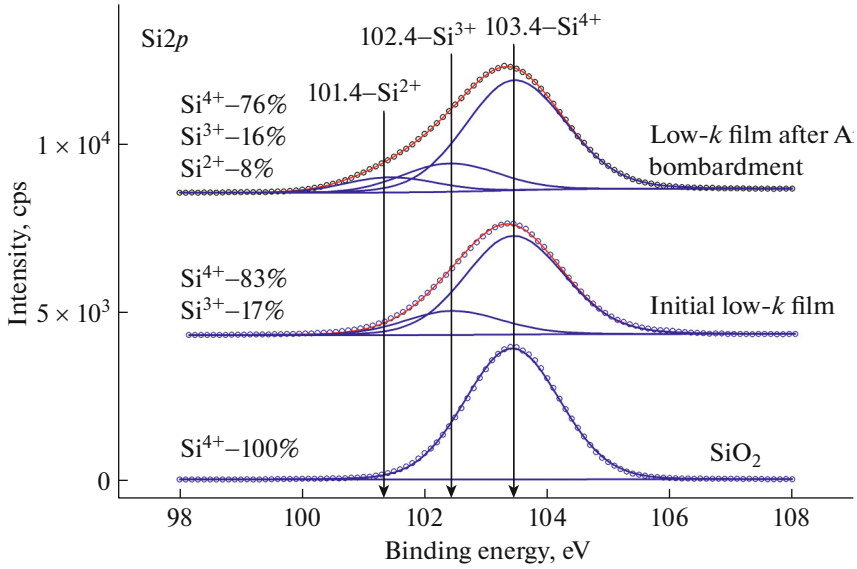

Fig. 2. XPS Si2*p* spectra and the deconvolution of thermally grown SiO_2, and low-*k* dielectric film before and after the Ar^+ ion bombardment.

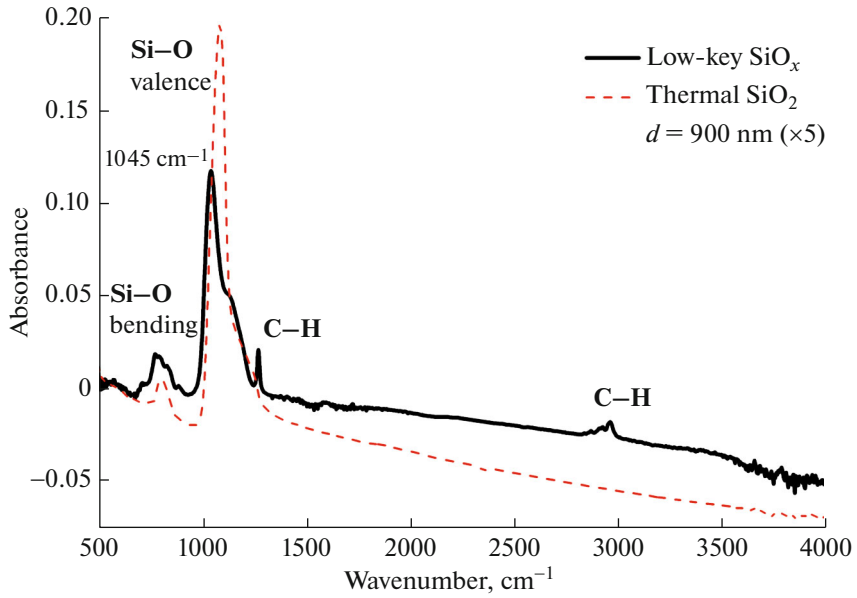

Fig. 3. FTIR absorption spectra of the low-*k* dielectric film and thermally grown SiO_2 film for comparison.

Figure 3 shows the FTIR absorption spectra of low-*k* dielectric film and thermally grown SiO_2 film for comparison. The Si substrates without films were used as reference samples during FTIR measurements in both cases. One can see that the spectrum of low-*k* dielectric film is dominated by the main lines at about 1045 and ~800 cm^{-1} which are ascribed to the Si–O–Si valence (stretching) and bending modes in the SiO_x films [15, 16], consequently. Position of Si–O–Si valence mode in SiO_2 film obtained by thermal oxidation of silicon (red dashed line) is shifted to higher frequencies (for convenience, this spectrum is divided by 5). As expected, it suggests that low-*k* film contains a higher concentration of silicon suboxide ($x < 2$) in comparison with thermal oxide [17]. According to data of Pai et al. [16] and Gambaryan at al. [18] that the position of this peak (in inverse centimeters) in SiO_x films almost linearly depends on the stoichiometric parameter x, approximately as:

$$\nu(\text{Si–O–Si stretching mode}) = 925 + 75x. \quad (1)$$

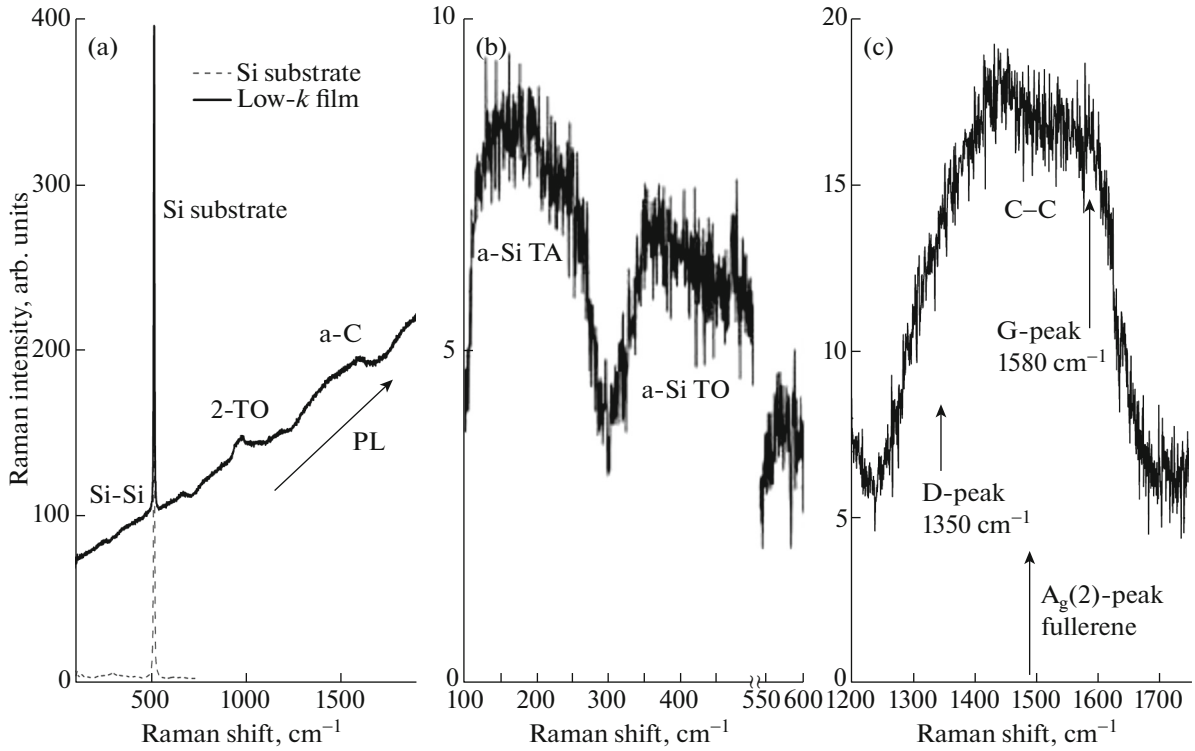

Fig. 4. Raman spectra of the low-*k* dielectric film and Si substrate. (a) All range; (b) range of Si–Si bonds vibrations; (c) range of C–C bonds vibrations.

The position of Si–O–Si valence mode peak in low-*k* dielectric film (solid black curve, Fig. 3) is 1045 cm^{-1}. So, according to equation (1), the stoichiometric parameter *x* in low-*k* dielectric film can be equal to 1.6. Of course, it should be noted that the presence of pores and carbon can also influence the vibration frequency of Si–O–Si valence mode. FTIR spectra also show pronounced peaks associated with the presence of C–H bonds ~1275 cm^{-1} (rocking mode) from $Si-CH_3$ groups originated from DEMS precursors [17]. These groups provide the films hydrophobicity important for dielectric properties. Several C–H related vibrations have contribution to absorption in the region 2800–3000 cm^{-1}. They can mainly be attributed to the following vibrations: antisymmetric (2968 cm^{-1}) and symmetric (2906 cm^{-1}) stretching vibrations of $C-H_3$ and also to antisymmetric (2916 cm^{-1}) and symmetric (2880 cm^{-1}) of $C-H_2$ stretching vibrations [17].

Figure 4a displays the Raman spectrum of low-*k* dielectric film together with a reference spectrum measured from a virgin Si (001) substrate. Unfortunately, the analysis of the Raman spectrum is complicated by the fact that it contains an intense background from photoluminescence (PL). One can see also some peculiarities at ~950 cm^{-1} related to 2-phonon scattering by transverse optical (TO) phonon in Si substrate.

Therefore, Figs. 4b, 4c show the spectra without the PL background (the line was subtracted from the initial spectrum). In Fig. 4b, the spectrum of Si substrate was also subtracted from the spectrum of the film. In Fig. 4b, one can see the broad bands at 350–500 and 100–250 cm^{-1} associated with the TO and transverse acoustic (TA) phonons, respectively, of amorphous Si [19]. Of course, the density of vibrational states of local silicon-silicon bonds in SiO_x films differ from the density of vibrational states in amorphous silicon, but there are qualitative coincidences—there are two regions of maximum density of states in the "optical" and "acoustic" ranges. It can be concluded that there are local Si–Si bonds in the studied low-*k* SiO_x films like in SiN_x films [20].

In Fig. 4c, one can see two broad bands, which can be associated with C–C vibrations—D and G peaks [21]. The observation of these peaks indicates the presence of both $s-p^3$ and $s-p^2$ hybridized C–C bonds [21]. It should also be noted that manifestation of PL with a maximum in the yellow-red range indicates the presence of amorphous carbon clusters [22, 23]. The existence of carbon clusters was observed earlier in films deposited from metal-organic precursors [23]. The presence of carbon in low-*k* dielectric films was also confirmed earlier by Marsik with co-authors from analysis of absorbance [24] and by Afanas'ev with co-authors from the analysis of the results of spectroscopy

of electron paramagnetic resonance on dangling carbon bonds [25]. It should be noted that the observed broad band may also be due to the signal from disordered fullerenes. It is known that the frequency of the most intense $A_g(2)$ mode from fullerenes is 1465 cm^{-1} [26]. Disordering can widen this band. Disordered fullerenes can also produce red photoluminescence.

To analyze the uniformity of the deposited low-k film thickness, scanning laser ellipsometry studies were applied; for this purpose the central 80 × 80 mm^2 region of the silicon wafer (300 mm in diameter) with the film was mapped with 1 mm (x) and 2 mm (y) steps. The laser beam was focalized into 10 μm light spot with the high-quality non-polarizing microobjective. The ellipsometer was designed with computer-operated scanning stage that allows measuring optical parameters distribution over sample surface up to 150 × 150 mm^2.

The measured spectra were used further to solve the inverse problem of ellipsometry and fit the calculated spectral dependences of ellipsometric angles Ψ and Δ to the experimental ones in accordance with the basic equation of ellipsometry:

$$\tan\Psi e^{i\Delta} = \frac{R_p}{R_s}, \qquad (2)$$

where R_p, R_s are the complex light reflection coefficients for the waves polarized in the incidence plane and perpendicular to it, depending on the optical constants and film thickness (one-film on substrate model was applied).

Figures 5a, 5b show 2D scans of thickness, d and refractive index (n) for the low-k dielectric film on Si substrate, correspondingly. As the data in Fig. 5 show, the values of the film thickness are in the range: 218–223 nm with an average value of ~220.5 nm, the refractive index: 1.355–1.380 (average volume ~1.367). So, Figs. 5a, 5b show a high homogeneity in thickness (~2.5%) and refractive index (~2%) of the low-k dielectric films.

The spectral dependences of the polarization angles in the whole spectral range for m points of the spectrum were fitted by minimizing the error function:

$$\sigma^2 = \frac{1}{m}\sum_{i=1}^{m}[(\Psi_{exp} - \Psi_{calc})^2 + (\Delta_{exp} - \Delta_{calc})^2], \qquad (3)$$

where Ψ_{exp}, Δ_{exp} and Ψ_{calc}, Δ_{calc}—experimental and calculated values of ellipsometric angles Ψ and Δ, respectively.

For ellipsometric calculations, an optical model of a single-layer reflecting system was also used. It was assumed that low-k dielectric film was isotropic and did not have gradients of optical characteristics and thicknesses. The calculations showed slight absorption of light in low-k films in the whole scanning spectral region ($\alpha(E) \neq 0$). Taking this fact into account, the thickness of the films and $n(E)$ spectral dependences were calculated basing on the Cauchy polynomial functions [27, 28]:

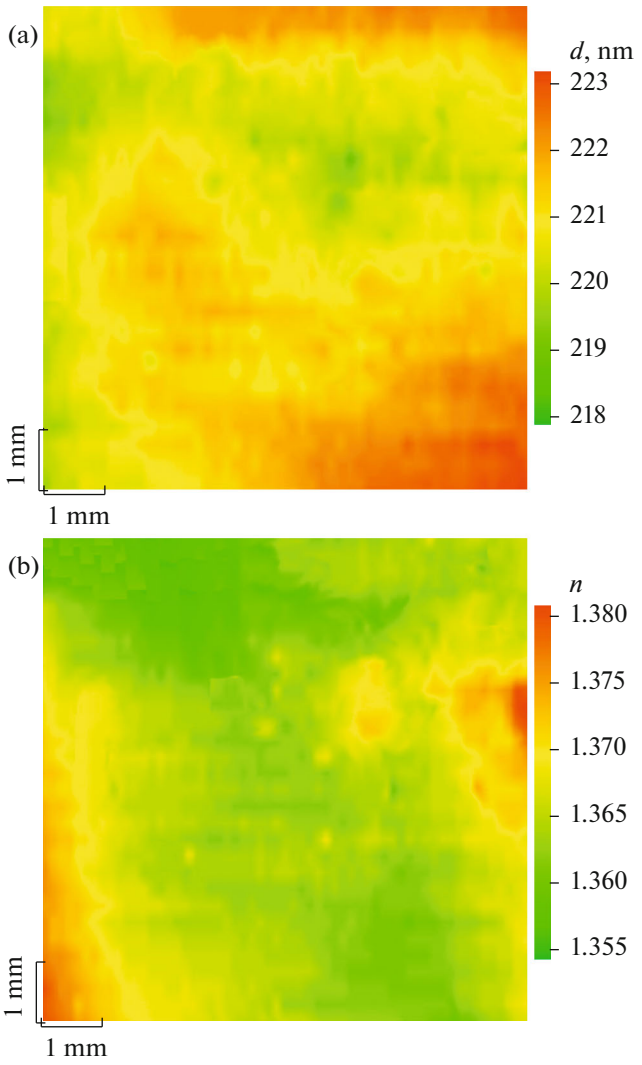

Fig. 5. Ellipsometric scanning of thin low-k film surface. Results of solution of the reverse ellipsometric problem: (a) thickness of the film, d; (b) refractive index of the film, n.

$$n(E) = a + bE^2 + cE^4, \quad k(E) = d + eE^2 + fE^4, \qquad (4)$$

where a, b, c, d, e, f are coefficients that were fitted to minimize the parameter σ in Eq. (3).

For calculations, the optical characteristics of silicon are taken from [29]. A four-zone measurement technique was used followed by averaging over all zones.

Thickness in each scanning point of the thin low-k film was calculated independently by solving of numerical-inversion problem of ellipsometry [28] for a simple optical model: Si—low-k dielectric—air.

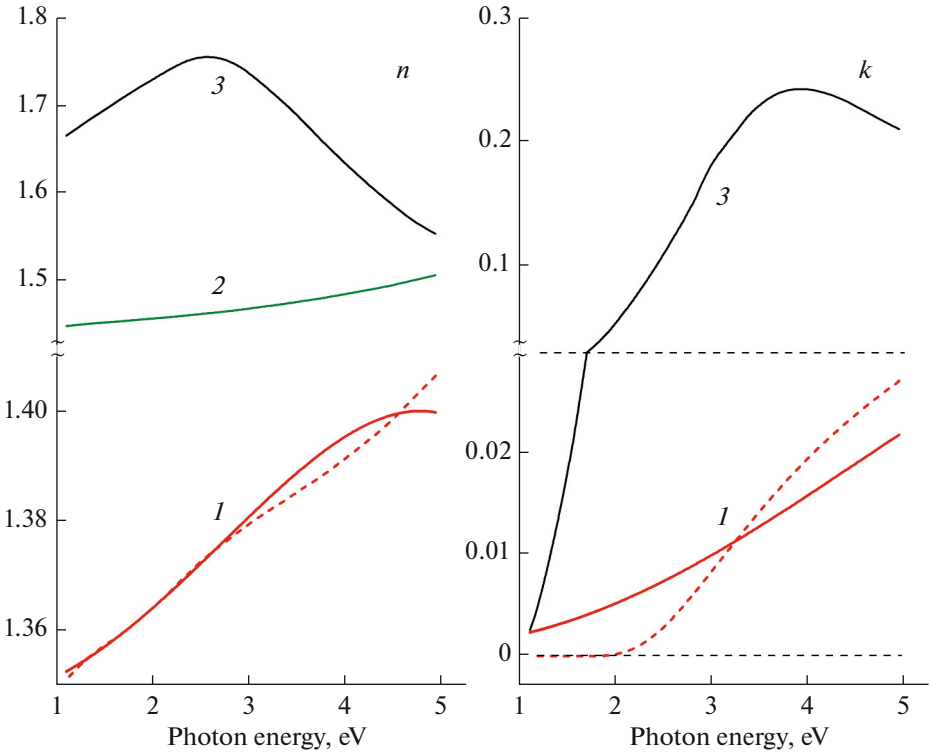

Fig. 6. Dependences of real, n (left side) and imaginary, k (right side) parts of complex refractive index ($N = n - ki$) on photon energy for films: *1* (red), thin low-k (solid lines—experiment, dashed lines—result of model calculation according to Bruggemann model, see text). *2* (green), thermal SiO_2, and *3* (black), amorphous carbon [27].

To estimate the fraction of amorphous carbon clusters, presumably causing absorption in the film, we used the Bruggemann effective medium model [27]:

$$\sum_i \left(q_i \frac{\varepsilon_i - \varepsilon_{\text{eff}}}{\varepsilon_i + 2\varepsilon_{\text{eff}}} \right) = 0, \qquad (5)$$

where q_i is part of the ith component of the mixture, ε_i, ε_{eff} are dielectric constants of the ith component and the effective medium. The appropriate components were chosen: silicon dioxide, amorphous carbon clusters, and voids [28]. The optical constant for amorphous carbon was taken from [30], also our clusters are not pure amorphous graphite, but there are no data on the optical constant of nano-inclusions with both s–p^3 and s–p^2 hybridized C–C bonds.

The dispersion dependences $n(E)$, $k(E)$ are normal and can be described by Cauchy polynomial functions (see Eq. (3)) with the coefficients: $a = 1.347$; $b = 4.651 \times 10^{-3}$; $c = -1.012 \times 10^{-4}$; $d = 0.001$; $e = 1.071 \times 10^{-3}$; $f = 0.09 \times 10^{-4}$. The thickness of the film was assumed to be 221.1 nm (see Fig. 5).

We assume that the main contribution to the absorption of the low-k dielectric is made by impurities of amorphous carbon formed during the decomposition of precursor substances. To estimate the possible carbon content, we performed an analysis using the Bruggemann effective medium model. It was assumed that the low-k dielectric layer includes: core material (presumably SiO_2), voids, and amorphous carbon. As a model material, we have chosen amorphous carbon with a high hydrogen content, which is most consistent with the chemical composition of the supposed impurities [30].

The best fit in the calculations according to the Bruggeman model was at the ratio of the components: SiO_2 ~69%, voids ~24%, amorphous carbon ~7% (see Fig. 6). $n(E)$, $k(E)$ dependences calculated with this estimate are shown in Fig. 6 by dash lines. The discrepancy in the dependences $n(E)$, $k(E)$, observed in the short-wavelength range ($E > 3$ eV), is possibly associated with the formation of large light-scattering carbon clusters and, thus, the inconsistency of the Bruggeman model.

So, the studied film is porous (which leads to a decrease in the dielectric constant), but contain Si–Si bonds, and also some amorphous carbon clusters (which leads to an increase in the dielectric constant). Absorption in the visible and near-UV spectral ranges is also possibly due to the presence of amorphous carbon clusters.

CONCLUSIONS

According to the analysis of spectral ellipsometry data in the frame of Bruggemann's effective medium theory, the investigated low-k dielectric is porous (porosity is about 24%), and contains amorphous carbon clusters (about 7%). Photoelectron, FTIR and Raman spectroscopies also indicate the presence of Si–Si bonds in the film. Irradiation by argon ion beam is accompanied by an increase of Si–Si bonds. According to Raman scattering data, the low-k dielectric contains amorphous carbon clusters, because C–C bonds are presented in the s–p^3 and s–p^2 hybridized forms. The presence of carbon clusters apparently leads to the absorption of light in the visible and near-UV ranges.

FUNDING

This work was supported by the Russian Foundation for Basic Research, project no. 18-29-27006. The Raman spectra were registered using the equipment of Center of collective usage "VTAN" in ATRC department of NSU.

CONFLICT OF INTEREST

The authors have declared no conflict of interest.

REFERENCES

1. R. H. Havemann and J. A. Hutchby, Proc. IEEE **89**, 586 (2001).
2. K. Maex, M. R. Baklanov, D. Shamiryan, F. Iacopi, S. H. Brongersma, and Z. S. Yanovitskaya, J. Appl. Phys. **93**, 8793 (2003).
3. M. R. Baklanov, K. Vanstreels, C. Wu, Y. Li, and K. Croes, in *Thin Films on Silicon* (Wiley, New York, 2016), Chap. 5.
4. A. Grill, Ann. Rev. Mater. Res. **39**, 49 (2009).
5. Z. Ming, H. Deng, S. Y. Xie, and B. Zhang, Mater. Sci. Semicond. Process. **39**, 235 (2015).
6. Z. Ming and B. Zhang, Mater. Sci. Semicond. Process. **36**, 170 (2015).
7. J. Moudler, W. Stickle, P. Sobol, and K. Bomben, *Handbook of X-ray Photoelectron Spectroscopy* (Perkin-Elmer, Eden Prairie, MN, 1992).
8. J. H. Scofield, J. Electron Spectrosc. Relat. Phenom. **8**, 129 (1976).
9. Software Informer. http://xpspeak.software.informer.com/4.1/.
10. T. V. Perevalov, A. A. Gismatulin, D. S. Seregin, Y. Wang, H. Xu, V. N. Kruchinin, E. V. Spesivcev, V. A. Gritsenko, K. A. Nasyrov, I. P. Prosvirin, J. Zhang, K. A. Vorotilov, and M. R. Baklanov, J. Appl. Phys. **127**, 195105 (2020).
11. E. V. Spesivtsev, S. V. Rykhlitskii, and V. A. Shvets, Optoelectron. Instrum. Data Process. **47**, 419 (2011).
12. S. V. Rykhlitskii, E. V. Spesivtsev, V. A. Shvets, and V. Yu. Prokopiev, Prib. Tekh. Eksp., No. 2, 161 (2012).
13. W. Zhang, S. Zhang, Y. Liu, and T. Chen, J. Cryst. Growth **311**, 1296 (2009).
14. A. Mehonic, M. Buckwell, L. Montesi, L. Garnett, S. Hudziak, S. Fearn, R. Chater, D. McPhail, and A. J. Kenyon, J. Appl. Phys. **117**, 124505 (2015).
15. G. Lucovsky, J. Yang, S. S. Chao, J. E. Tyler, and W. Czubatyj, Phys. Rev. B **28**, 3225 (1983).
16. P. G. Pai, S. S. Chao, Y. Takagi, and G. Lucovsky, J. Vacuum Sci. Technol. A **4**, 689 (1986).
17. A. Grill and D. A. Neumayer, J. Appl. Phys. **94**, 6697 (2003).
18. M. P. Gambaryan, G. K. Krivyakin, S. G. Cherkova, M. Stoffel, H. Rinnert, M. Vergnat, and V. A. Volodin, Phys. Solid State **62**, 492 (2020).
19. J. E. J. Smith, M. H. Brodsky, B. I. Crowder, and M. I. Nathan, Phys. Rev. Lett. **26**, 642 (1971).
20. V. A. Volodin, V. A. Gritsenko, and A. Chin, Tech. Phys. Lett. **44**, 424 (2018).
21. A. C. Ferrari and J. Robertson, Phys. Rev. B **61**, 14095 (2000).
22. J. Robertson, Phys. Rev. B **53**, 16302 (1996).
23. T. P. Smirnova, V. A. Volodin, M. S. Lebedev, and V. I. Belyi, Opt. Spectrosc. **110**, 55 (2011).
24. P. Marsik, P. Verdonck, D. de Roest, and M. R. Baklanov, Thin Solid Films **518**, 4266 (2010).
25. V. V. Afanas'ev, K. Keunen, A. Stesmans, M. Jivanescu, Zs. Tokei, M. R. Baklanov, and G. P. Beyer, Microelectron. Eng. **88**, 1503 (2011).
26. H. Kuzmany, R. Pfeiffer, M. Hulman, and C. Kramberger, Phil. Trans. R. Soc. London, Ser. A **362**, 2375 (2004).
27. H. Tompkins and E. A. Irene, *Handbook of Ellipsometry* (William Andrew, Springer, 2005).
28. P. M. Amirtharaj, *Handbook of Optical Constants of Solids,* Ed. by D. Palik (Elsevier, Amsterdam, 1991).
29. S. Adachi, *Optical Constants of Crystalline and Amorphous Semiconductors: Numerical Data and Graphical Information* (Springer Science, New York, 1999).
30. G. Compagnini, Appl. Phys. **33**, 7377 (1994).